Evolution of Anisotropies in Asymmetric Heavy Ion Collisions

A Senior Honors Thesis

Presented in Partial Fulfillment of the Requirements for graduation
with distinction in Physics in the undergraduate colleges
of The Ohio State University

by
Michael Wong

The Ohio State University
May 2009

Project Advisor: Dr. Ulrich Heinz, Professor, Department of Physics

Abstract:

Anisotropic expansion of Quark-Gluon Plasma fireballs created in heavy ion collisions at high energies is studied using relativistic hydrodynamic simulations. I quantify the asymmetry using Fourier coefficients in order to inspect the relation between deformations of the initial energy distribution and anisotropies of the finally measured momentum distributions.

Introduction:

The Relativistic Heavy Ion Collider provides a wealth of data for theorists to explain. This information is about emitted particles, so collision dynamics must be inferred. RHIC collisions are so energetic that atoms melt into a plasma of quarks and gluons which flows like an ideal fluid[1], surrounded by hadron gas, with a mixed-phase region in between[2]. Computer simulations predict observable features of the distribution of emitted particles based on a theoretical model which, together with initial collision geometry, determines the evolution of the fireball. My research is part of a search for further evidence for the hydrodynamic model.

We simplify our calculations using the initial collision geometry. Particle accelerators give heavy nuclei relativistic speeds along a *beam direction* while limiting their motion perpendicular to this direction. Though the beam path may be curved, it is locally linear on the scale of the nuclei. Certain quantities such as proper time are *invariant under longitudinal boosts*, so we can infer the status of the entire fireball from information about any plane perpendicular to the beam path. We define this *transverse plane* so that it also contains the relativistic center of mass of the collision. When we refer to a vector quantity such as momentum, we refer only to its component in this plane. The plane is oriented so that the colliding nuclei line up along the X axis, with the origin halfway between their centers (see Figure 1). This orientation makes all collisions symmetric about the X axis. Collisions between identical nuclei – *symmetric collisions* – are also symmetric about the Y axis. The distance between nuclear centers is *peripherality* (also known as *impact parameter*). Any collision at zero peripherality – any *central collision* – is *isotropic*, i.e. it has circular symmetry about the origin.

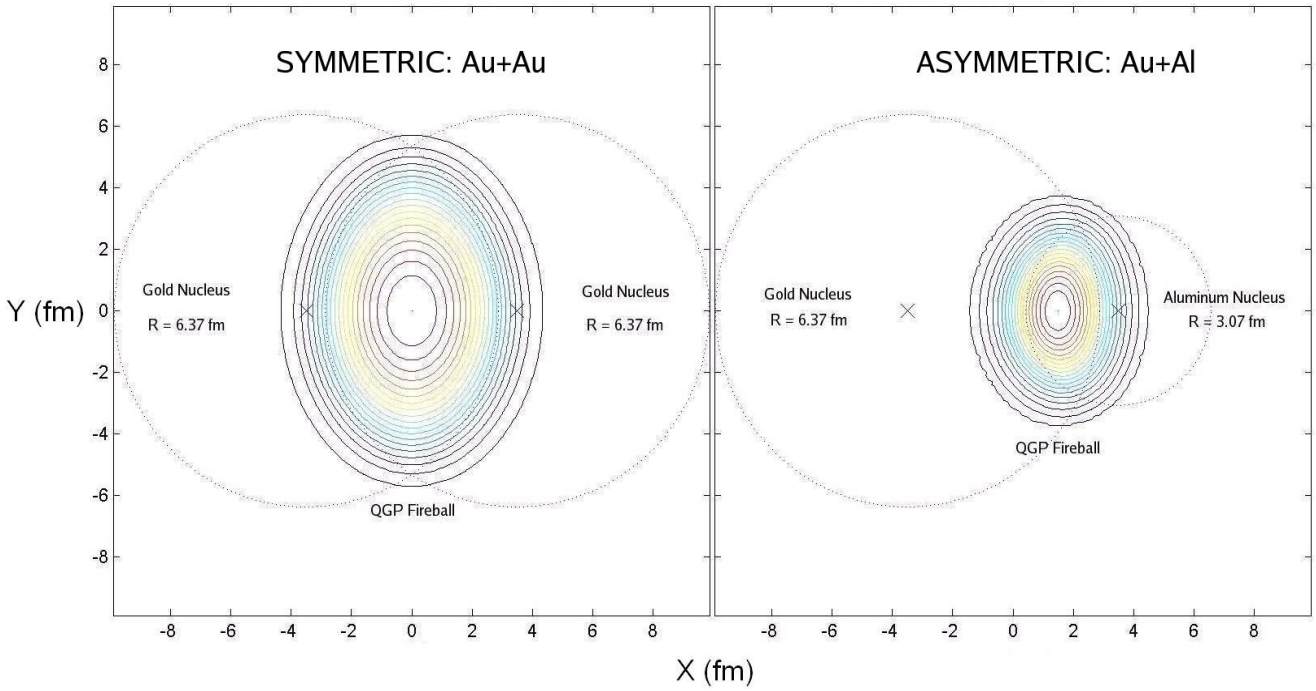

Figure 1: Initial energy density distributions in the transverse plane, with 7 fm peripherality.

One observable feature of the emitted particle distribution is its set of *anisotropies* – deviations from circular symmetry. Anisotropies in a distribution are quantified by a set of *Fourier coefficients*. Symmetric collisions create distributions whose odd Fourier coefficients vanish. Previous studies of symmetric collisions have found a definite causal relationship between the second coefficient for fluid energy density and corresponding coefficient for emitted particle momenta[3]. We studied asymmetric collisions so that additional anisotropies could be measured using the odd coefficients. The entire fireball is 'frozen out' into hadrons too quickly for experimental detectors to determine how the distributions evolve over time, so this information must be obtained indirectly (using theory) from other observables. I will use the evolving energy density as a proxy for time.

Methods:

Relativistic Hydrodynamic Simulation:

We track fluid parameters on a finite, discrete representation of the transverse plane – the plane containing the relativistic center of mass, perpendicular to pre-collision trajectories. Values at nonzero longitude can be determined from this by boost-invariance. Proper time begins counting from 0.6 fm/c because this is the experimentally measured time before the fluid achieves *local thermalization* – approximate temperature equilibrium at each point in the fluid – which is required for hydrodynamics

to apply. Initial energy density distributions are calculated as in [2] from the position, thickness function, and mass of each nucleus. Experimentally measured data determine the ratio of hard (wounded nucleon) to soft (binary collision) contributions, which set entropy density and baryon number density. From these distributions we use an *equation of state* to calculate pressure, temperature, energy density, and chemical potential. Different models of the phase transition correspond to different equations of state. EOS I represents uniformly QGP matter, while EOS Q allows a first-order transition, in thermal and chemical equilibrium, between QGP and hadron gas. The calculated values evolve over time according to discretized versions of the equations of relativistic hydrodynamics. Emitted gluon momentum is computed from temperature and fluid velocity distributions. The evolution of the distributions of energy density and emitted gluon momentum will be analyzed.

Fourier Decomposition:

We analyze distributions by decomposing them into Fourier coefficients. Fourier coefficients are weighted sums over the relevant distributions, where the weight depends on angle with respect to a center point. The Fourier coefficient of a generic two-dimensional distribution $f(r;\theta)$ is given by:

$$a_n = \frac{\int_0^{2\pi} \cos(n\theta) f(\theta)\, d\theta}{\int_0^{2\pi} f(\theta)\, d\theta}, \quad \text{where}$$

$$f(\theta) = \int_0^{\infty} f(r,\theta)\, r\, dr$$

We define ω_n as the nth spatial Fourier coefficient of the energy density distribution at any time t, where the energy density function $e(r;\phi,t)$ is given by hydrodynamic evolution:

$$\omega_n(t) = \frac{\int_0^{2\pi} \cos(n\phi) e(\phi,t)\, d\phi}{\int_0^{2\pi} e(\phi,t)\, d\phi}, \quad \text{where}$$

$$e(\phi,t) = \int_0^{\infty} e(r,\phi,t)\, r\, dr$$

The *nth* Fourier coefficient describes the amplitude of the nth harmonic of the angular anisotropy; when the distribution is balanced in every direction around its center point, they are all zero. We examine the first four Fourier coefficients because of their geometrical significance (see Figure 2).

Each of these coefficients is normalized by dividing by an unweighted sum over the distribution.

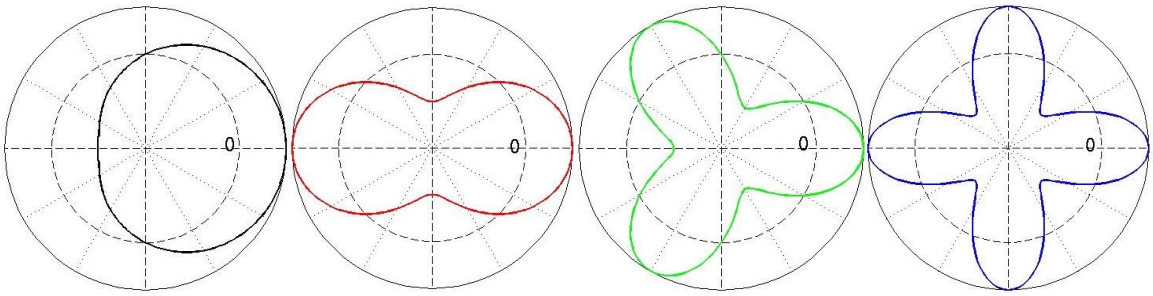

Figure 2a: Large 1st Fourier coefficient. *Figure 2b: Large 2nd Fourier coefficient.* *Figure 2c: Large 3rd Fourier coefficient.* *Figure 2d: Large 4th Fourier coefficient.*

The relativistic center of energy density is a natural center point for heavy ion collisions because it is fixed in space by conservation of energy and momentum. The center of energy density is defined by:

$$\vec{R} = \frac{\int e(\vec{r})\,\vec{r}\,dA}{\int e(\vec{r})\,dA}, \quad \text{where}$$

$$\text{relativistic:} \quad e(\vec{r}) = T^{oo}c^2$$

$$\text{nonrelativistic:} \quad e(\vec{r}) = \epsilon(\vec{r})$$

ϵ and T^{oo} are both given by the hydrodynamic equations; c is the speed of light. The difference between relativistic and classical centers grows to almost 2% as large as the values themselves for Au+Al (see Figure 3), so it is important to distinguish between the two. The gradual drift in the relativistic center of energy density in our simulation is an error, but only amounts to about 0.3% of the value. We verified that this 0.3% error negligibly affects the Fourier coefficients calculated with respect to this point by comparing their evolution when calculated with respect to fixed and drifting centers, reproducing Figure 6 and Figure 7 below.

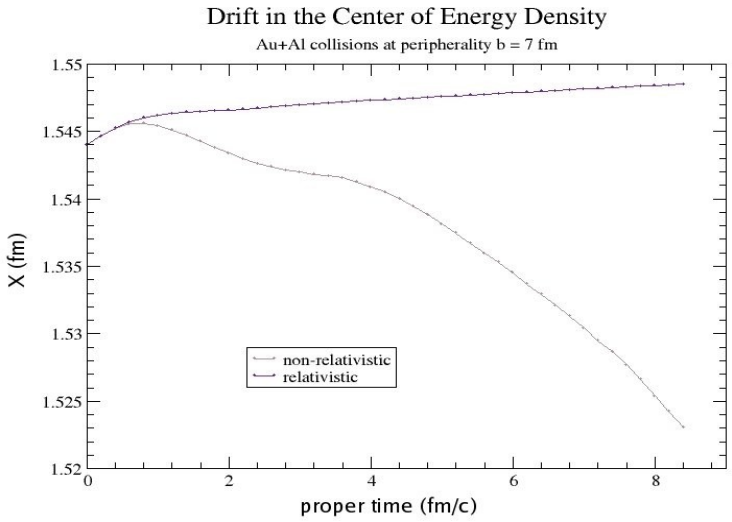

Figure 3: Time evolution of the X-coordinate of the center of energy density (Y-coordinate is zero). Proper time is adjusted by thermalization time (τ_o = 0.6 fm/c).

Connection to Observables:

We consider the evolution of the collision in terms of energy density. Experiments measure the energy of emitted particles, but heavy ion collisions occur too quickly to clock the creation of particles. Moreover, the types and distributions of emitted particles depend on the state of matter, which is determined by energy density. Therefore, it is over a series of energy densities that we track the distributions, which form a set of space-time surfaces (see Figure 4). Phase transformations occur at critical energy density values; throughout the collision, energy density tends to decrease as the fireball expands. In Au+Al collisions at 7 fm peripherality, the center of mass is not the last point to cool into the mixed phase even though it is the last to freeze out of that state. The reverse is true of Au+Au. This inequality between energy density at the center of mass and peak energy density yields two slightly different parametrizations of the evolution of the fireball.

We calculate each surface of constant energy density using the time-evolution of a two-dimensional energy density distribution. We first determine the grid points bounding the surface: we identify every square on the transverse plane with corners on opposite sides of the threshold energy density. We then look at this square and the square prior to it in time, forming a square prism in space-time, and perform a three-dimensional linear interpolation to estimate a point on the constant-energy surface. We take time steps of 0.04 fm/c with spatial gridline separation of 0.1 fm (in both directions) throughout the simulation. A typical horizontal (constant-time) slice of a constant energy surface

corresponds to one contour on a contour plot such as Figure 1, but some horizontal slices create multiple contours for the same energy.

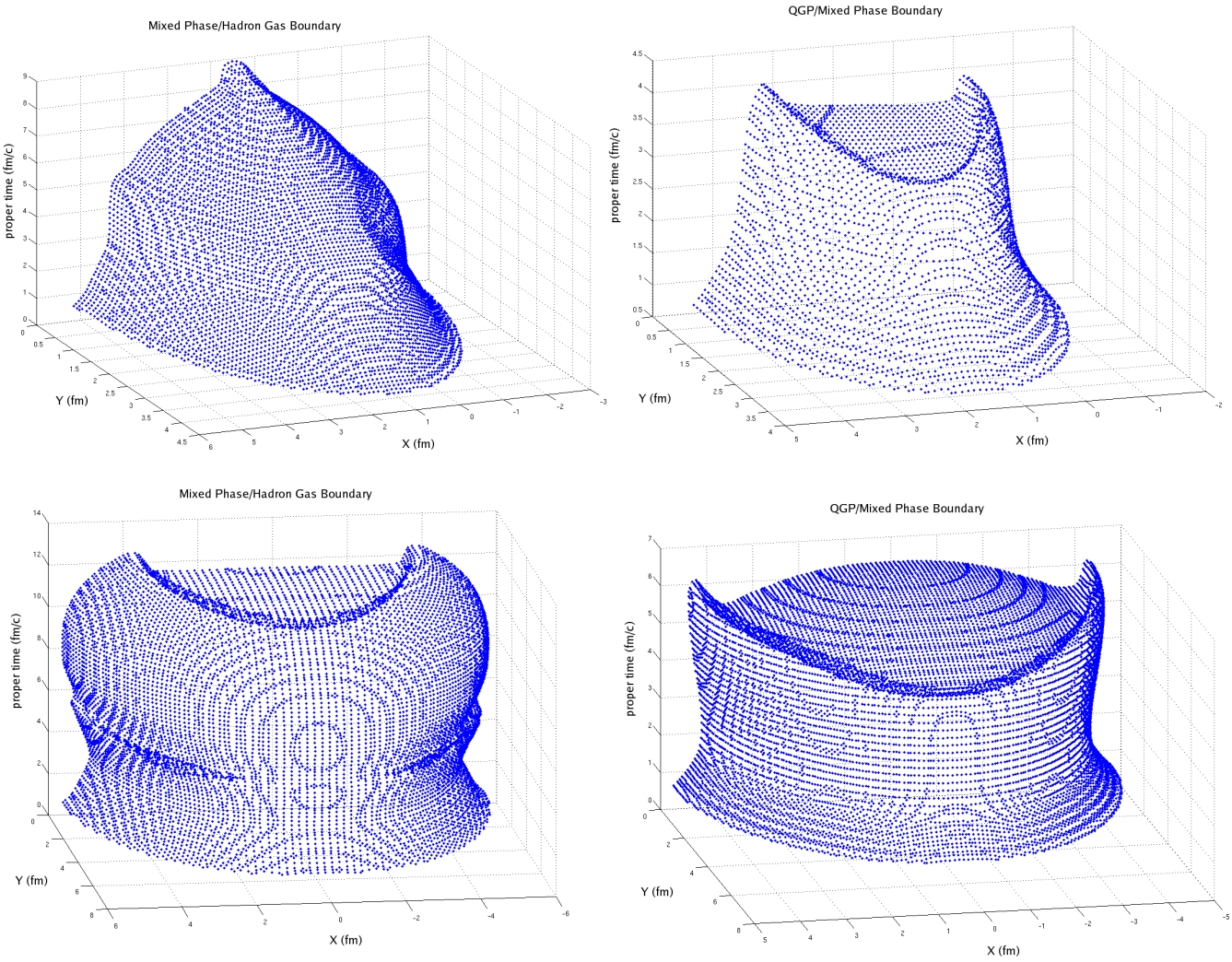

Figure 4: Space-time surfaces of constant energy density e = 0.075 (left) and e = 0.45 (right) GeV/fm³, for Au+Al (top) and Au+Au (bottom), at 7 fm peripherality.

As a proxy for time, we use the logarithm of energy density. This variable decreases with time, so we use the opposite of this logarithm, i.e. the logarithm of a *reciprocal* (see Figure 5). We normalize the energy density e by its initial value e_o at the center of energy density. Figure 5 compares the time when the fireball center passes through the energy density versus the latest time of *any* point on the surface corresponding to this energy density (these times may differ - see Figure 4). We see that both times are approximately linear functions of $ln(e_o/e)$ with decreasing slope. This implies that energy density at the fireball center decreases over time with an approximate power law, where the power decreases somewhat over time. This relationship is not true for complete freezeout since the slope

jumps discontinuously near $\ln(e_o/e) = 4.3$, so we use the center of mass parametrization.

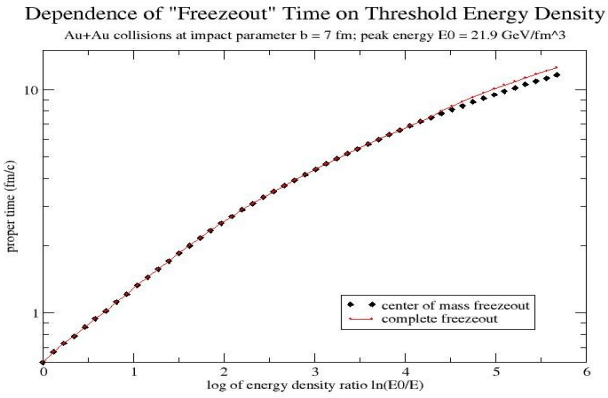

Figure 5: The amount of time the fireball takes to descend below (freeze out) energy density e.

In order to understand the evolution of anisotropies with respect to energy density, we must extend the definition of Fourier coefficients to quantify anisotropy at constant energy density rather than constant time. The distribution is now a surface with three dimensions (two spatial plus one time), so the *n*th momentum-space Fourier coefficient, of energy density, on constant-energy surface $\Sigma(e)$, is:

$$\omega_n(e) = \frac{\int_{\Sigma} \cos(n\phi) u^{\mu} d^3\sigma_{\mu}}{\int_{\Sigma} u^{\mu} d^3\sigma_{\mu}}$$

u^{μ} is the relativistic four-velocity of the fluid and $d^3\sigma_{\mu}$ is a relativistic volume element. We also define v_n as the *n*th momentum Fourier coefficient of the emitted gluon momentum distribution, where $n(p,\varphi,e)$ is the number density distribution in p-space of gluons that would be emitted if freezeout occurred at energy density *e*:

$$v_m(e) = \frac{\int_0^{2\pi} \cos(m\phi) n(\phi, e) d\phi}{\int_0^{2\pi} n(\phi, e) d\phi}, \quad \text{where}$$

$$n(\phi, e) = \int_0^{\infty} n(p, \phi, e)\, p\, dp$$

We calculate the distribution function as in [2] and [4]:

$$n(p, \phi, e) = \frac{1}{(2\pi)^3} \int_{\Sigma(e)} f(\vec{r}, \vec{p})\, p^{\mu} d^3\sigma_{\mu} = \frac{dN}{dy\, pdp\, d\phi}(p, \phi, e), \quad \text{where}$$

$f(\vec{r}, \vec{p}) = \frac{1}{e^{p^\mu u_\mu(\vec{r})/T(\vec{r})} \pm 1}$ is the phase-space distribution function.

p^μ is the relativistic four-momentum and T is temperature.

Results:

Evolution of Anisotropies:

I plot Fourier coefficients for both energy density and emitted gluon momentum distributions against the logarithm of the reciprocal of energy density, for both EOS I and EOS Q (see Figure 6). The second coefficient dominates both distributions; it is so large for the momentum distribution that I plot it using two different vertical axis scales. All momentum coefficients fluctuate near $\ln(e_o/e) = 2.2$, for EOS Q but not EOS I, representing the phase transition. The second coefficient decreases during this transition because the mixed phase cannot support large pressure gradients [5]. The phase transition has little effect on the spatial coefficients.

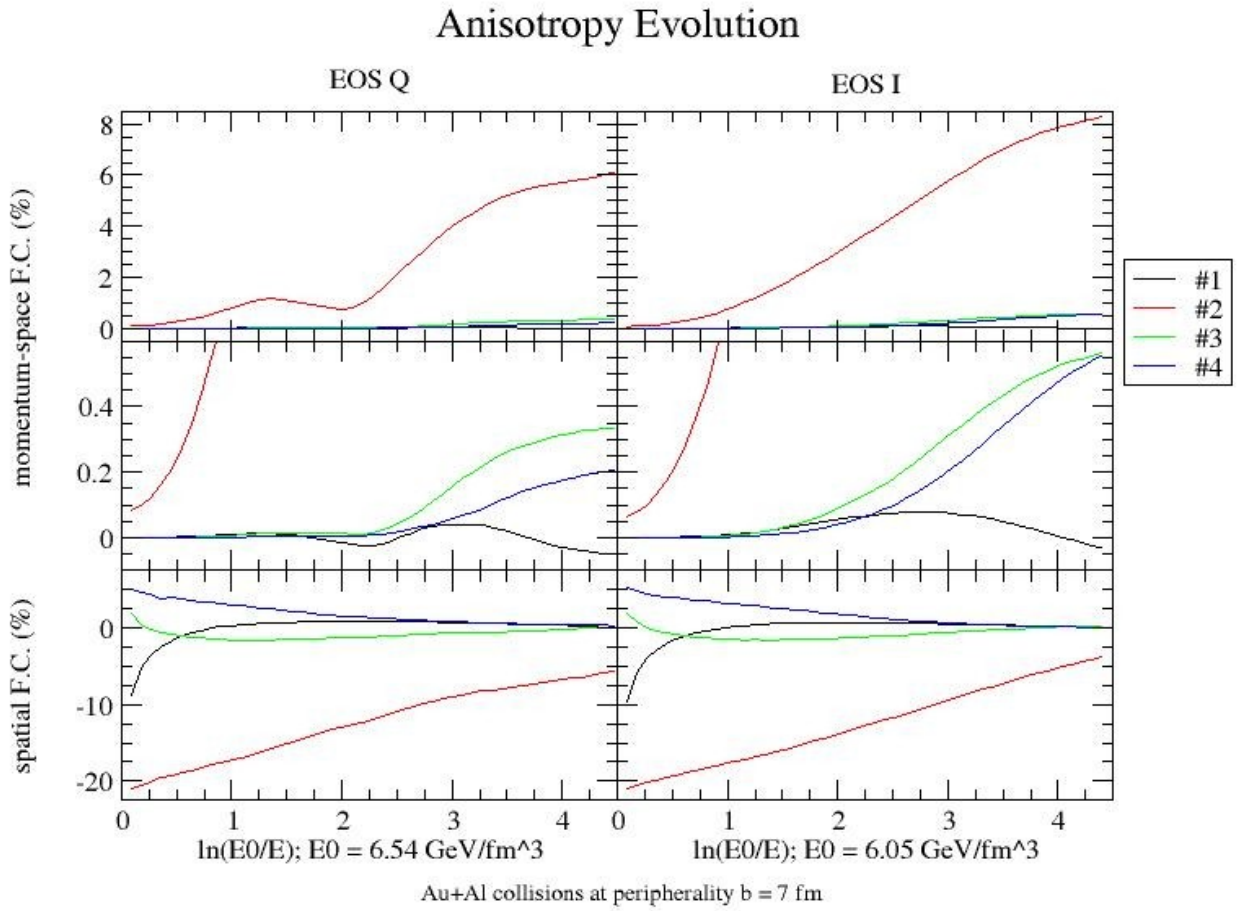

Figure 6: Spatial energy density anisotropies and momentum-space density anisotropies as functions of the logarithm of the reciprocal of energy density.

I plot the time evolution of the spatial energy density Fourier coefficients ω_n (Figure 7) for comparison to the energy-evolution plots (Figure 6). The second coefficient dominates both. The collision freezes out before 3.5 fm/c for the plasma of EOS I, while the gradual phase transition prolongs it to over 8 fm/c for EOS Q. I also plot the initial anisotropy in energy density and entropy density distributions against peripherality to illustrate the dependence of anisotropies on collision geometry (see Figure 8). Anisotropies of the energy and entropy distributions are remarkably similar at thermalization. As expected, the second coefficient grows larger in absolute value, and remains negative, as the collision zone becomes thinner (higher peripherality). The fourth coefficient is positive and also grows in absolute value with increasingly peripheral collisions, and then all coefficients level off before peripherality approaches the sum of the atomic radii (9.44 fm for Au+Al), the maximum peripherality for collisions to occur at all.

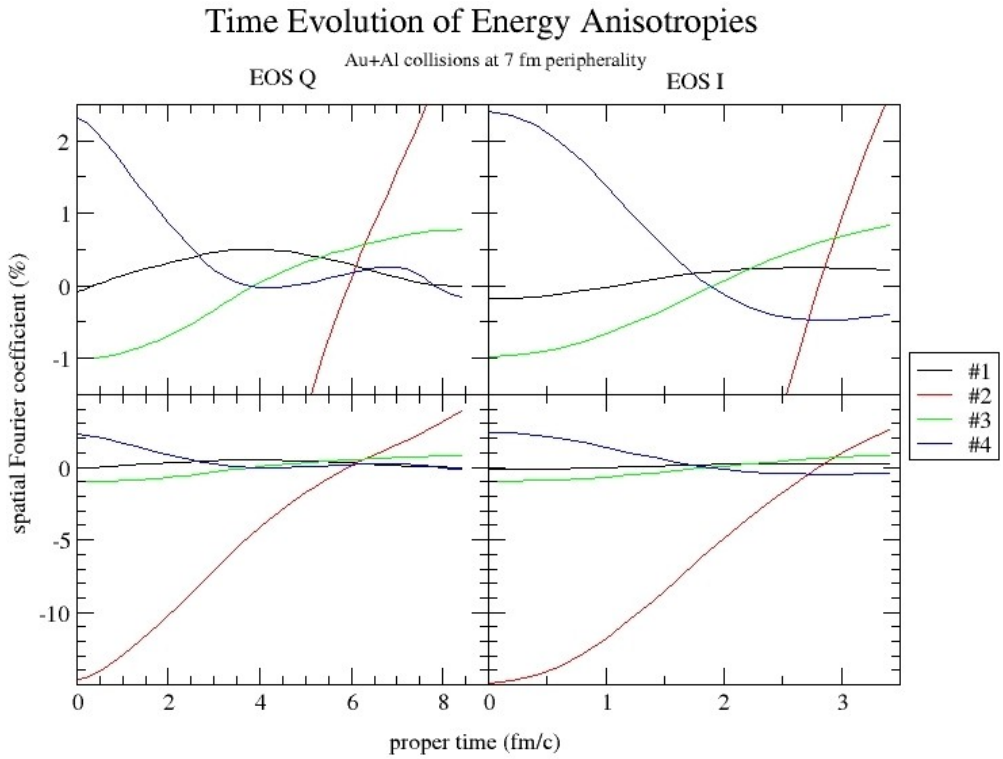

Figure 7: Spatial energy density Fourier coefficients as functions of proper time. Proper time is adjusted by thermalization time (τ_o = 0.6 fm/c).

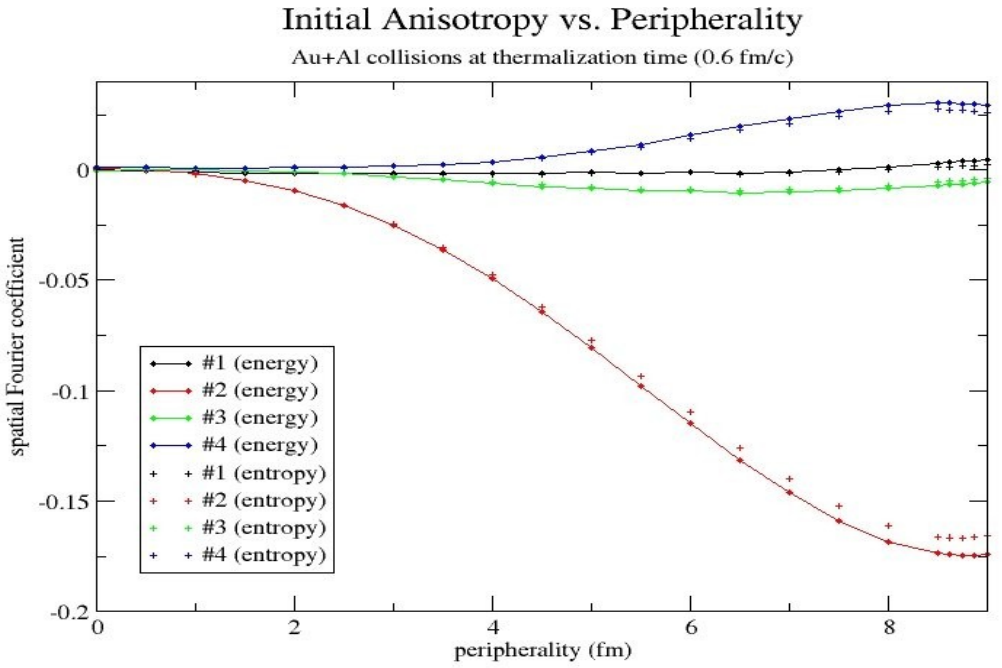

Figure 8: Spatial energy and entropy density Fourier coefficients as functions of peripherality, at thermalization.

I also calculate the momentum coefficients as functions of momentum for EOS Q (see Figure 9). Since emitted particle momentum doesn't depend merely on energy density, then this relationship supplies additional information about the momentum distribution which can be experimentally verified. The second coefficient dominates at all momenta and increases almost linearly with momentum.

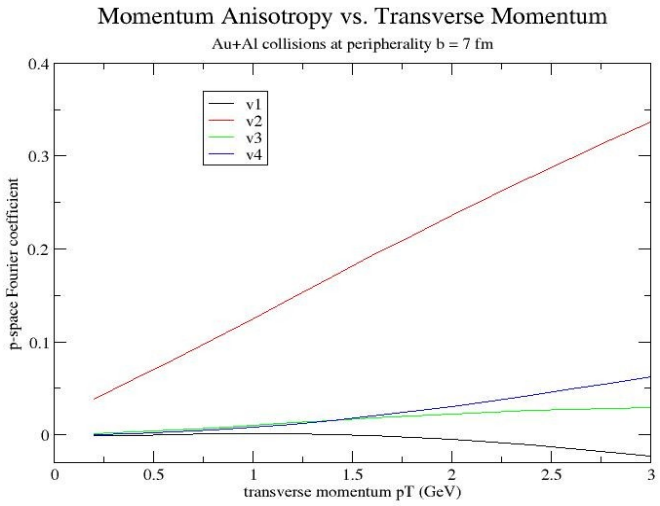

Figure 9: Momentum-space Fourier coefficients as functions of momentum.

Conclusions:

I have made a quantitative prediction of the observable evolution of anisotropies in the momentum distribution of emitted gluons for Au+Al at 7 fm peripherality (Figure 6), which is also a qualitative prediction for asymmetric collisions with similar geometry. I generalized our simulation program to make predictions for asymmetric collisions, in case such collisions should be performed at RHIC or LHC. Should they involve nuclei other than Au+Al, at any peripherality, a simple tweak of initial conditions will now generate a testable prediction of the hydrodynamic model. Though this study focused on emitted gluons, the same techniques and software can be used to calculate momentum anisotropies for various particles. Further research might determine causal links between anisotropies (besides the second coefficient) in the spatial energy density and emitted particle momentum.

References:

[1] H. Song and U. Heinz, Physical Review C **77**, 064901 (2008).

[2] P. F. Kolb, J. Sollfrank, and U. Heinz, Physical Review C **62**, 054909 (2000).

[3] P. F. Kolb, Physical Review C **68** 031902 (2003).

[4] U. Heinz, P. F. Kolb, hep-ph/0204061 (2002).

[5] P. F. Kolb and U. Heinz, in *Quark-Gluon Plasma 3* (World Scientific, Singapore, 2004, edited by R. C. Hwa and X. N. Wang), p. 673–714.